Science and Technology Indonesia
e-ISSN:2580-4391 *p*-ISSN:2580-4405
Vol. 9, No. 1, January 2024

Research Paper

Synthesis and Characterization of CuO and NiO Nanoparticles Derived from Schiff Base Complexes

Ali Taleb Bader[1*], Nada Ahmed Rasheed Al-qasii[2], Asmaa Mohammed Noori Khaleel[2]

[1]*Department of Chemistry, College of Sciences for Woman, University of Babylon, Hilla, 51001, Iraq*
[2]*Department of Chemistry, College of Science, University of Baghdad, Baghdad, 11001, Iraq*
***Corresponding author**: wsc.ali.taleb@uobabylon.edu.iq

Abstract
This study reports the synthesizes of such as copper oxide (CuO) and nickel oxide (NiO) nanoparticles (NPs) by thermal decompositions of Schiff base complexes and their physical characterization. A polydentate Schiff base ligand, (E)-2-(((2-chlorobenzyl)imino)methyl)phenol (CIMP), was synthesized by condensing 2-chlorobenzylamine and 2-hydroxybenzaldehyde. The ligand was identified by melting point, FT-IR, UV-Vis, and (^{1}H and ^{13}C NMR) spectroscopy. Cu(II) and Ni(II) complexes were prepared by reacting CIMP with the corresponding molar ratio in a 1:1 (metal: ligand). The complexes (Com1 and Com2) were characterized by melting point, FT-IR, and UV-Vis spectroscopy. The FT-IR spectra of the (Com1 and Com2) showed that the deprotonated CIMP ligand coordinated to the Ni(II) and Cu(II) metal ions through the azomethine nitrogen, aryl chloride, chlorine, and phenolic oxygen atoms. To determine the crystalline structure of the synthesized products, X-ray powder diffraction (XRD) and scanning electron microscopy (SEM) techniques were employed. The formation of copper oxide and nickel oxide as the new products was confirmed by XRD analysis. SEM imaging revealed the uniform and spherical morphology of the nanoparticles, which exhibited a remarkably narrow size distribution with an average diameter of 20 to 22 nm, highlighting their exceptional precision.

Keywords
Nanoparticles, Schiff Base Complexes, Thermal Decomposition

Received: 8 September 2023, Accepted: 4 December 2023
https://doi.org/10.26554/sti.2024.9.1.103-112

1. INTRODUCTION

In the past three decades, "Schiff bases and their metal ion complexes" have been synthesized. This has garnered significant attention from numerous research groups. These compounds exhibit versatile properties and have been employed in a wide range of applications in catalytic industrial processes (Hossain et al., 2022). A variety of structures and functionalities can be achieved by Schiff bases, which are formed by condensing aldehydes or ketones with primary amines. These compounds have been extensively studied due to their coordination chemistry with various metal ions that result in the formation of metal complexes with fascinating properties. For example, copper Schiff base complexes have shown promising catalytic activity in organic transformations, such as C–C bond formation and oxidation reactions (Tsacheva et al., 2023). Similarly, nickel Schiff base complexes have shown useful in homogeneous catalysis, such as cross-coupling reactions and carbon-carbon bond activation (Kuchtanin et al., 2016).

A thermal decomposition method is more suitable Schiff bases metal ion complexes because it facilitates the process conditions, particle size, crystal structure, and purity (Elseman et al., 2016; Ghaffari et al., 2014; Khalaji, 2013; Ourari et al., 2014; Sumalatha et al., 2023). Moreover, the metal complexes derived from Schiff bases can be further transformed into their respective metal oxides, which exhibit unique physicochemical properties and have various applications. Copper oxide (CuO) and nickel oxide (NiO) are two prominent examples of metal oxides that are derived from Schiff base complexes. CuO nanoparticles (NPs) have been utilized as catalysts in a various kinds reactions, such as the oxidative degradation of organic pollutants and CO oxidation (Ibrahim et al., 2018).

Nanotechnology is focused on the manipulation and production of nanoscale particles and included the capability of measuring, visualizing, manipulating, and manufacturing objects at the atomic or molecular level, typically ranging from 1 to 100 nm. Moreover, nanotechnology has revolutionized fields such as computing, and has facilitated advances in nanodiodes and nanotransistors. Compared to conventional technologies, nanotechnology has also contributed to the development of lighter, more durable, and stronger batteries, fuel cells, and

solar cells (Parveen et al., 2016). Metal oxide nanostructures, in particular, have garnered considerable attention because of their properties and promising implementation in a large variety of applications spanning optoelectronics, optics, catalysis, sensors, and electronics (Abu-Dief and Mohamed, 2017; Abu-Dief et al., 2016; Ali and Abu-Dief, 2015; Jia et al., 2009). Among the diverse range of metal oxides, CuO stands out as a narrow band gap semiconductor, boasting a mere 1.2 eV. This distinctive attribute positions CuO as an intriguing candidate for various applications, including optoelectronic devices, catalytic processes (Bayansal et al., 2011). Similarly, NiO nano particulars excels semiconductors with a relatively broad band gap of 3.6 eV, offering exciting possibilities in areas such as supercapacitor devices, lithium-ion microbial fuel cells, gas sensing, and photocatalytic reduction of methyl orange dye in ethanol, and for addressing challenges related to nitrogen dioxide. These features contribute to the inclusion of NiO in the pantheon of versatile materials (Salavati-Niasari et al., 2009a). The remarkable potential of these metal oxide nanostructures opens up a realm of possibilities for advancements in numerous fields. Moreover, thermal decomposition techniques have emerged as highly promising methods for the synthesis of metal oxide nanostructures Because they are capable of controlling the particle size, particle crystal morphology, and purity of particles (Farhadi and Roostaei-Zaniyani, 2011; Salavati-Niasari et al., 2009a; Salavati-Niasari et al., 2009b).

Additionally, these techniques offer several advantages, including shorter processing times, higher yields, lower costs, and reduced power consumption. In the present study, the tridentate Schiff base ligand(CIMP) in metal ion complexes acts as a coordination entity via its oxygen, nitrogen, and chlorine atoms, as determined by various analytical methods, including "ultraviolet-visible (UV-Vis), Fourier transform-infrared (FT-IR), and ^{1}H, and ^{13}C-nuclear magnetic resonance (NMR) spectroscopies". The thermal decomposition process of the ligand complexes unveils the exquisite Ni(II) and Cu(II) oxide nanostructures, thereby harnessing the inherent advantages of this method. The synthesized NiO and CuO nanoparticles (NPs) were fully characterized using, "FT-IR, X-ray powder diffraction (XRD), energy-dispersive X-ray (EDX) spectroscopies and scanning electron microscopy (SEM)". The synthetic methods employed in the present study enabled us to maintain meticulous control over the process conditions, particle size, and particle crystal structure, while also allowing for lower calcination temperatures and enhancing the purity of the products to unprecedented levels. CuO and NiO nanoparticles, derived from metal ion complexes, offer exciting prospects for various applications. The use of thermal decomposition techniques enables precise control over the synthetic process, resulting in nanostructures with tailored properties and enhanced performance (Refat et al., 2022; Singh et al., 2023).

2. EXPERIMENTAL SECTION

2.1 Materials

The chemical compounds were of high purity and used without further purification, including salicylaldehyde (Merck, Germany), 2-chlorobenzylamine (Merck), nickel acetate tetrahydrate $Ni(CH_3COOH)_2.4H_2O$, and copper acetate hydrate $Cu(CH_3COOH)_2$. H_2O (BDH, England).

2.2 Instruments

To determine the melting points, we used a Stuart digital melting point apparatus, SMP30. This state-of-the-art instrument facilitates the precise and accurate recording of melting points. We used FT-IR spectroscopy to analyze the molecular structures and functional groups with a Shimadzu FT-IR spectrophotometer (model: Broker Spectrophotometer), spanning a spectral range of 4000 to 400 cm^{-1}. These analyses were conducted on KBr disks, providing invaluable insights into the chemical compositions of the compounds under examination. The UV-Vis spectra, which provided information on the absorption characteristics of the compounds, were measured using a Shimadzu UV-Vis Spectrophotometer, model 1700. Operating at room temperature (r.t. ˚C), we employed a 1 cm quartz cell to enable the examination of UV-Vis spectra within the range of 200 to 1100 nm. A sample concentration of 10-3 M in dimethylformamide (DMF) as a solvent was meticulously chosen to ensure the precision of our measurements. Furthermore, we probed the structural elucidation of the ligand through the acquisition of ^{1}H and ^{13}C NMR spectra. The spectra were recorded using a Bruker DMX-400 spectrophotometer, operating at 400 MHz. The solvent employed for the NMR studies was deuterated dimethyl sulfoxide (DMSO-d6). This commonly used solvent in NMR spectroscopy enabled us to glean valuable insights into the molecular architecture and bonding patterns of the ligand.

2.3 Methods

2.3.1 Preparation of the Schiff Base Ligand(CIMP)

The preparation of the Schiff base compound was based on a previously reported method (Phurat et al., 2010). In this technique, 2-chlorobenzylamine (5 mL, 0.035 mole) was added to a stirred ethanol solution containing salicylaldehyde (5 mL, 0.035 mole). After that, the reaction mixture was shaken for 4 hours under refluxing conditions. Following this process, the mixture was allowed to rest at room temperature, resulting in the formation of yellow crystals, as illustrated in Scheme (1). In summary, the Schiff base compound was synthesized using a method previously described in the literature (Phurat et al., 2010). The reaction involved the addition of 2-chlorobenzylamine to a stirred ethanol solution of salicylaldehyde, followed by refluxing for 4 hours. After being left to stand at room temperature (RT), the resulting mixture yielded yellow crystals.

© 2024 The Authors.

2.3.2 Synthesis of the Com1 and Com2 Metal Ion Complexes

The transition metal complexes are synthesized, and separate solutions of metal ion salts $Ni(OAc)_2{\cdot}4H_2O$ and $Cu(OAc)_2{\cdot}H_2O$ were prepared by dissolving 0.004 mol (1.06 g) and 0.004 mol (0.85 g) of each metal salt, respectively, in 20 ml of distilled water. A hot ethanol solutions of the Schiff base ligand (1 g, 0.004 mol) was gradually added to each of the metal salt solutions while stirring continuously. The mixture was refluxed for 5 hours to enhance the precipitation of the metal complexes, as shown in Scheme 1. Finally, to ensure the purity and stability of the synthesized metal complexes, the final products were thoroughly dried in an oven, a critical step in their preparation (Kargar et al., 2021).

2.3.3 Synthesis of the NiO and CuO Nanoparticles

The Schiff base complexes were carefully placed in crucibles and subsequently placed in an oven. The oven temperature was incrementally raised by 10°C every minute in the presence of air. After 4 hours of heating, nanoparticles of NiO and CuO were obtained at a temperature of 500°C. To ensure purity, the final products were thoroughly washed with ethanol to remove any impurities. The nanoparticles were subsequently left to dry at RT for many hours. The chemical structure of the synthesized NiO and CuO nanoparticles is shown in Scheme 1 (Kargar et al., 2021).

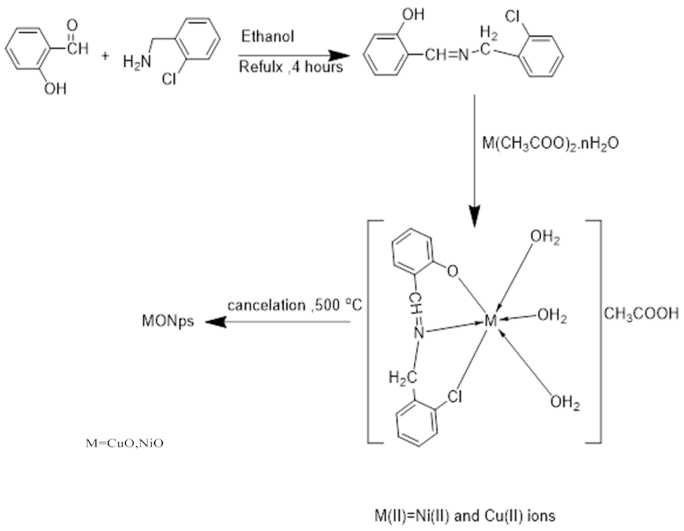

Scheme 1. Synthesizes of the Ligand (CIMP), (Com1 and Com2) Metal Ion Complexes, and Metal Oxide Nanoparticles (MONps)

3. RESULTS AND DISCUSSION

3.1 FT-IR Spectra of the Ligand, Metal Ion Complexes, and Metal Oxide Nanoparticles

The functional group vibrations observed by FT-IR for the starting materials, the Schiff base ligand, the metal ion complexes, and metal oxide (NiO and CuO) NPs are listed in Table 1 and shown in Figures 1 and 2. The Ligand (CIMP) display distinct azomethine and OH frequencies around (1600-1640) cm^{-1} and (2500-3100) cm^{-1}, respectively, (Silverstein et al., 2005). In the spectrum of the metal ion complexes were founded , the azomethine band shifts to a lower range of frequencies due to N-atom involvement in the C=N group (Devi et al., 2023; Nakamoto, 2009). The deprotonation is caused by the interaction of the hydroxyl group with the metal ions, leading to the formation of metal–O bonds and the subsequent loss of the proton from the hydroxyl group. In the ligand spectra, strong bands around 745 cm^{-1} indicate the participation of the halide group in the coordination of the complex. In the spectra of the metal ion Ni(II) and Cu(II) metal complexes, these bands shift to approximately 756 cm^{-1}, indicating coordination with the metal. Figure 2 shown the (CIMP) ligand spectra show strong bands around 450 cm^{-1}, indicating the halide group were coordinated through metal ions . However, in the spectra of the metal ion complex, these bands shift to approximately 745 cm^{-1}, which suggests coordination of the halide group with the metal ion. This shift in wavenumber denotes the formation of a new M–X bond, where X represents the halide ligand, with the bands emerging at around 450 cm^{-1} and 360 cm^{-1} in the metal complex IR spectra, which likely corresponds to the M–O and M–N bond formations, respectively (Nakamoto, 2009). The results of the Schiff base complexes suggest that chelation leads to a decrease in the wavenumber of the C=N bands. When organic ligands are coordinated with metal ions, their IR spectra show shifts similar to those seen when ligands are absorbed onto salt substrates. Therefore, both scenarios can be treated similarly (Kargar et al., 2021; Parashar et al., 1988). Nanoparticles of CuO and NiO were further characterized by FT-IR. The stretching vibrations of Cu–O were attributed to a prominent absorption band in the FT-IR spectrum. On the other hand, NiO nanoparticles typically exhibit an absorption band between 450 and 550 cm^{-1}. The peak observed at 420 cm^{-1} in the spectrum unequivocally confirms the presence of crystalline NiO and was specifically assigned to Ni–O stretching (Yang et al., 2013).

3.2 Electronic Spectra of the Ligand (CIMP) and its (Com1 and Com2) Metal Ion Complexes

Figure 3 shows the electronic transitions spectra of the ligand and the metal complexes in DMF. As a result of intra-ligand transitions, a highly intense singlet band emerges in the electronic spectrum of the (CIMP) ligand. Notably, the band observed at 268 nm (37313.43 cm^{-1}) was assigned to the π-π* transition of the conjugated system, while a secondary band with reduced intensity appeared at (315 nm, 31746.03 cm^{-1}) and was designated as the n-π* transition. These intriguing spectra are depicted in Figure 3. In the electronic transitions spectra of the nickel ion complex, four absorption bands were observed at the following wave numbers and wavelengths, respectively: 640 nm (15625 cm^{-1}), 415 nm (24096.39 cm^{-1}), 340 nm (29411.76 cm^{-1}), and 272 nm (36764.71 cm^{-1}). The octahedral shape and possible D4h symmetry of the complexes

© 2024 The Authors.

Table 1. FT-IR Spectra: Reagents (2-hydroxybenzadehyde, 2-chlorobenzylamine), Ligand-Metal Complexes, and Characterization of the Metal Oxide Nanoparticles (NPs)

Compound	υ(C=O) cm^{-1}	$\upsilon(NH_2)$ Asym-sym cm^{-1}	υ(CH=N) cm^{-1}	υ(O−H) cm^{-1}	υ(C−Cl) cm^{-1}	υ(M−O) cm^{-1}
2-hydroxybenzaldehyde	1660	- - - - -	- - -	3190-3045	- - - -	- - - - -
2-chlorobenzylamine	- - - - -	3302-3370	- - - - -	- - - -	745	- - - -
Schiff Base (Ligand)	- - - -	- - - -	1633	3095	745	- - - -
Ni(II) Schiff Base Complex	- - -	- - - -	1613	- - -	756	458
Cu(II) Schiff Base Complex			1621	- - - -	756	460
NiO NPs	- - - -	- - - - -	- - - - -	- - - - -	- - - - -	461
CuO NPs						480

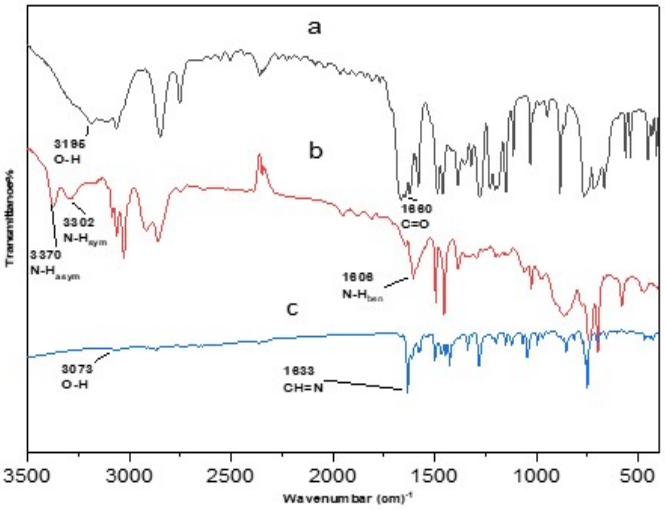

Figure 1. FT-IR Spectra of (a) 2-hydroxybenzaldehyde, (b) 2-chlorobenzylamine, and (c) Schiff Base Ligand

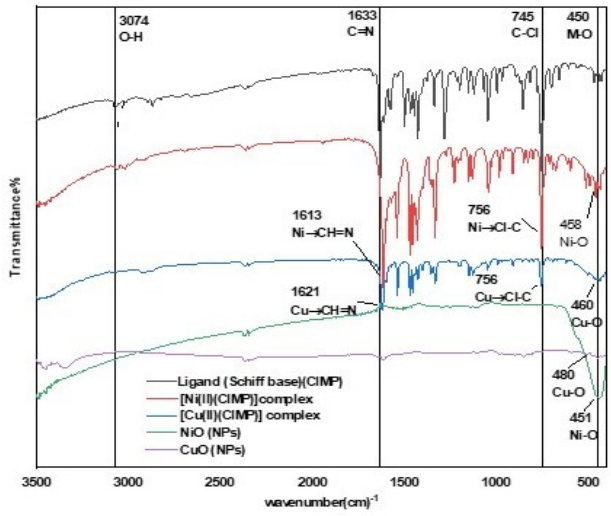

Figure 2. FT-IR Spectra of the Schiff Base Ligand (CIMP) and its Metal Ion Ni(II) and Cu(II) Complexes and Nanoparticle Oxides (NiO and CuO)

are revealed by a thorough examination of these bands. The three spin-allowed shifts that these bands correspond to are: $^3A_2g(F) \rightarrow {}^3T_1g(F)$ ($\upsilon 2$), $^3A_2g(F) \rightarrow {}^3T_1g(P)$ ($\upsilon 3$), and metal-to-ligand charge transfer (MLCT), respectively, based on the ^3A_2g ground state of Ni(II) in an octahedral geometry environment (Chandra and Gupta, 2004; Gopalan, 2001; Turner, 2002). The copper (II) complexes show absorption bands at 638 nm (15673.98 cm^{-1}) and 375 nm (26666.67 cm^{-1}), which indicate a square planar structure and can be attributed to the transitions "$^2B1g \rightarrow {}^2B_2g$ and $^2B_1g \rightarrow {}^2E_g$," respectively. Moreover, a band at 280 nm (35714.29 cm^{-1}) is due to MLC (Singh and Kumar, 2006; Turner, 2002).

3.3 ^{1}H-NMR Spectra Characterizations

The ligand's and its metal complexes' molecular structures were confirmed. by the 1H-NMR spectra, which are shown in Table 2 and Figure 4. The spectra were recorded in DMSO-d^6 with TMS as an internal standard. The protons were identified by their distinct chemical shifts and coupling patterns. The results suggested the following structure for the complexes (Devi et al., 2022; Silverstein et al., 2005). The absence of any shift in the signals of the azomethine and hydroxy protons in the metal ion (Com1 and Com2) complexes indicated that these groups were involved in metal coordination (Jeewoth et al., 2000).

3.4 ^{13}C-NMR Spectra for Characterizing the Schiff Base Ligand

The carbon nuclear magnetic resonance spectral data of the Schiff base ligand are shown in Figure 5 and Table 3 and provide additional support for the composition of the ligand. The molecular structure of the Schiff base ligand, based on the findings from the spectrum of the chemical shifts, is shown in Table 3 (Santhi et al., 2023; Silverstein et al., 2005).

© 2024 The Authors.

Table 2. ^{1}H-NMR Data for the Schiff Base Ligand

H/C	Chemical Shift (δ)	Interpretation	References
-δOH	13.3 ppm	Singlet due to (OH) of phenolic proton	(Devi et al., 2022; Yousif et al., 2017)
δCH=N	8.7 ppm	Singlet due to CH=N of azomethane	(Yousif et al., 2017)
δ(8H)	6.8-7.5 ppm	Multiplet due to the aromatic protons	(Silverstein et al., 2005)
δ(2H)	4.8 ppm	Signal due to $-CH_2$ in the ligand	(Silverstein et al., 2005)
δ(DMSO)	2.5 ppm	Signal for the solvent DMSO	(Devi et al., 2022)
$\delta(H_2O)$	3.4 ppm	Signal for water	(Silverstein et al., 2005)

Table 3. ^{13}C-NMR Data for the Schiff Base Ligand

C/H	Chemical Shift (δ) ppm	Interpretation	References
CH_2	60 ppm	due to CH_2 from benzalamine	(Silverstein et al., 2005; Devi et al., 2022)
C=N	160 ppm	Due formation imine group C=N for Schiff base	(Yousif et al., 2017; Silverstein et al., 2005)
(C-aromatic)	δ=116-136 ppm	due to the aromatic carbons	(Silverstein et al., 2005)
δ(DMSO)	40 ppm	for the solvent	(Silverstein et al., 2005)

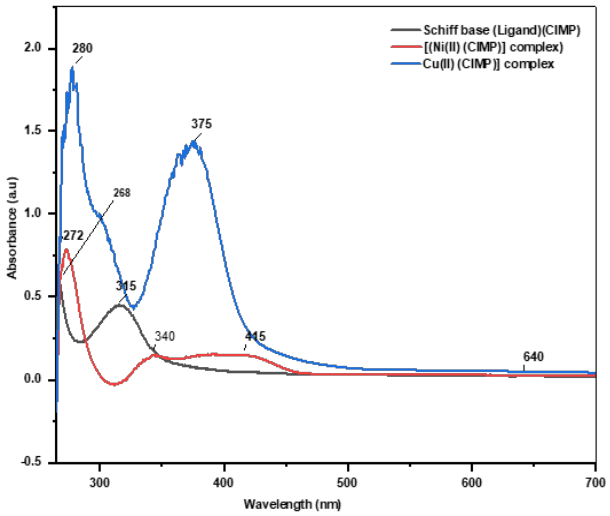

Figure 3. Electronic Spectra of the Ligand (CIMP) and its Metal Ion (Com1and Com2) Complexes

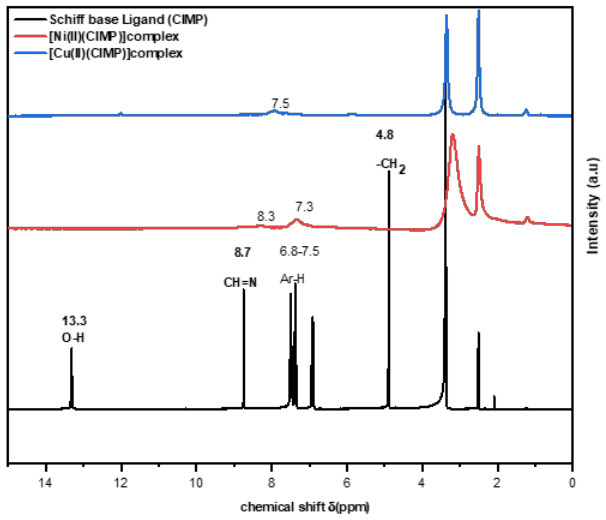

Figure 4. ^{1}H-NMR Spectra of the Ligand and (Com1 and Com2) Complexes

3.5 X-Ray Diffraction Analysis of the Metal Ion Schiff Base Complexes and Metal Oxide Nanoparticles

The crystalline phase of the (Com1 and Com2) complexes is evident from the sharp peaks in their powder XRD patterns, which are displayed in Figure 6 for the range (2θ = 0–80°). Using Scherer's formula, the average crystallite size of the complexes was estimated and found to be 39.8 nm and 30.7 nm, respectively. The XRD pattern of the NiO nanoparticles following calcination at 500°C is shown in Figure 7. The discernible peaks exhibited by the pattern align harmoniously with the Bragg reflections of the face-centered cubic structure. The maxima of the three strong Bragg's peaks are located at 2θ = 37.28°, 43.29°, and 62.91°, respectively. The cubic structure of NiO corresponds to the Joint Committee on Powder Diffraction Standards (JCPDS), card number 00-001-1239. The detected peaks of diffraction that match the planes are (111), (200), and (220) (Jassim et al., 2023). The average crystallite size of the NiO nanoparticles was determined to be 26.72 nm, using the Debye-Scherrer formula, which involves analyzing the broadening of the X-ray diffraction lines (Gobinath et al., 2023; Patterson, 1939).

In addition, the XRD pattern revealed the nature of the

© 2024 The Authors.

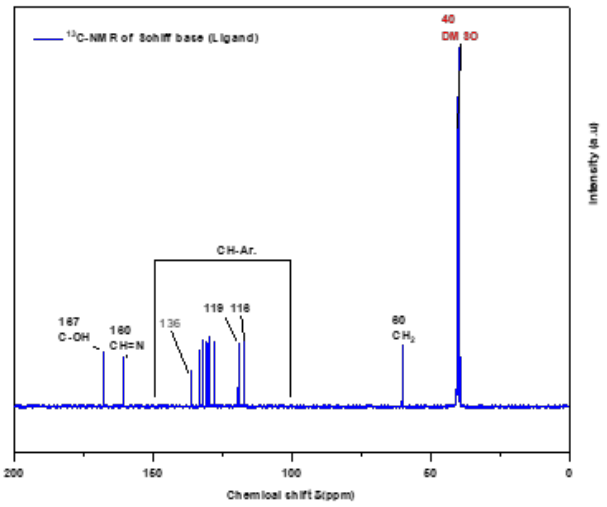

Figure 5. ^{13}C-NMR Spectra for the Schiff Base Ligand

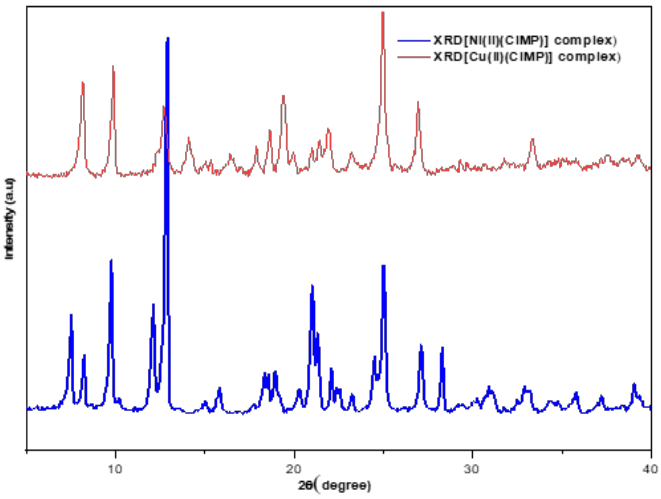

Figure 6. XRD Pattern of the (Com1and Com2) Complexes

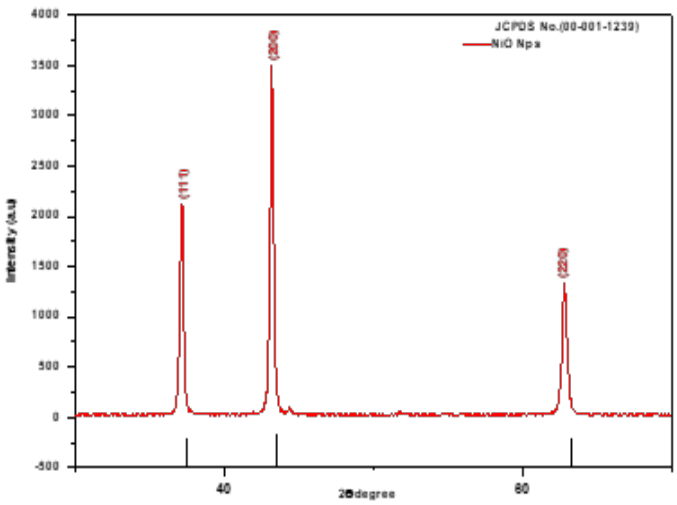

Figure 7. XRD Pattern of the NiO Nanoparticles and JCPDS No. 00-001-1239

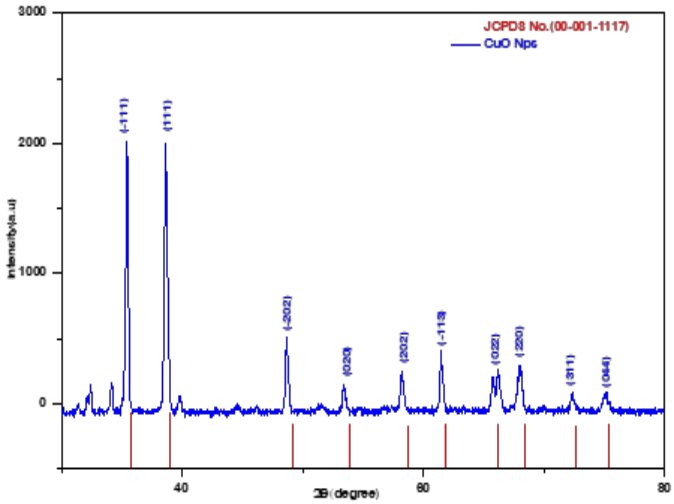

Figure 8. XRD Pattern of the CuO Nanoparticles and JCPDS No. 00-001-1117

CuO products post-calcination at 500°C. The diffraction peaks showcased in this pattern align perfectly with the monoclinic structure of copper oxide, as indexed in the JCPDS database with the reference number 05-0661, as shown in Figure 8. The peaks are approximately positioned at the 2θ values of 35.43°, 38.66°, 48.70°, 53.39°, 58.25°, 61.17°, 67.95°, 72.39°, and 75.11° and indicate the (-111), (111), (-202), (-202), (020), (202), (-113), (022), (220), (311), and (044) crystal planes, respectively. This harmonic arrangement of crystal planes accentuates the inherent attractiveness of the CuO nanoparticles and showcases their structural characteristics (Dabhane et al., 2023). The Debye-Scherer equation was used to estimate the average size of the nanoparticles from the FWHM of the diffraction peak, the X-ray wavelength, and Bragg's angle. The CuO nanoparticles were found to have an average size of about 26.7 nm, revealing their nanoscale features shown in Equation 1.

$$D = \frac{K\lambda}{\beta \cos\theta} \quad (1)$$

- D: The size of the crystals we want to find out
- K: A number that depends on the shape of the crystals (usually around 0.9)
- λ: The wavelength of the X-rays we use to scan the crystals
- β: The width of the X-ray peak at half of its maximum height
- θ: The angle at which the X-rays bounce off the crystals

We found out the size of the tiny crystals of NiO that formed when we heated them up to 500°C. Impressively, these

© 2024 The Authors.

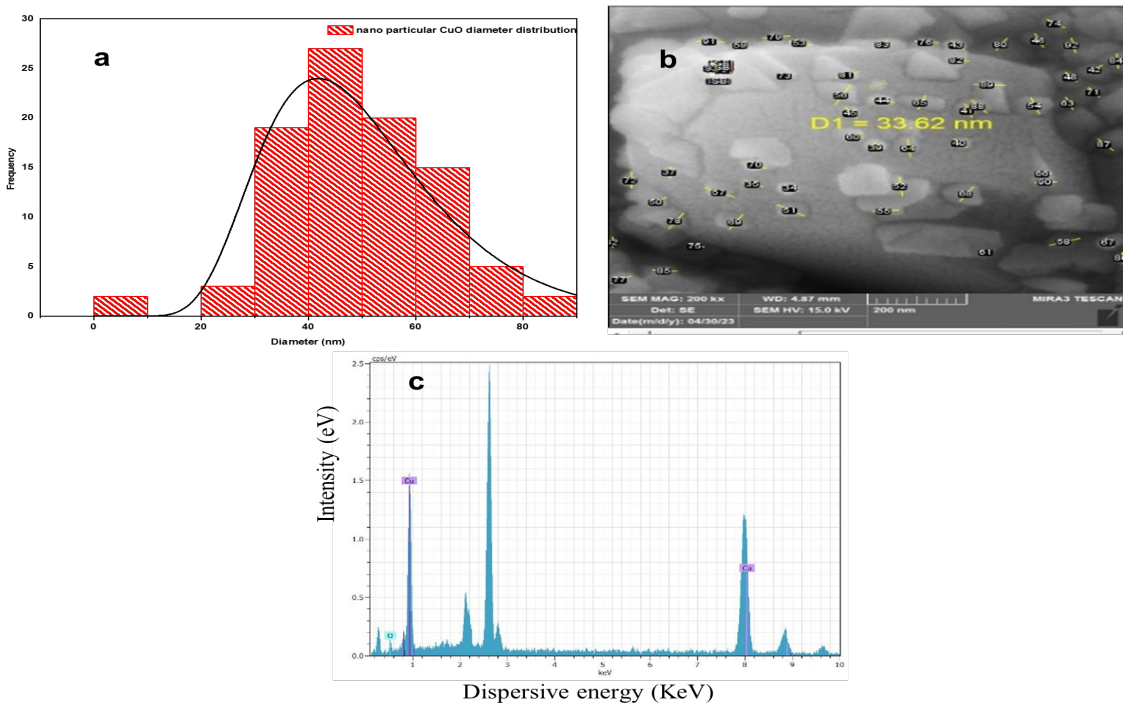

Figure 9. (a) Distribution Curve for the CuO Nanoparticles (b) SEM Image of CuO Nanoparticles and C-EDX Spectra for CuO Nps (c)

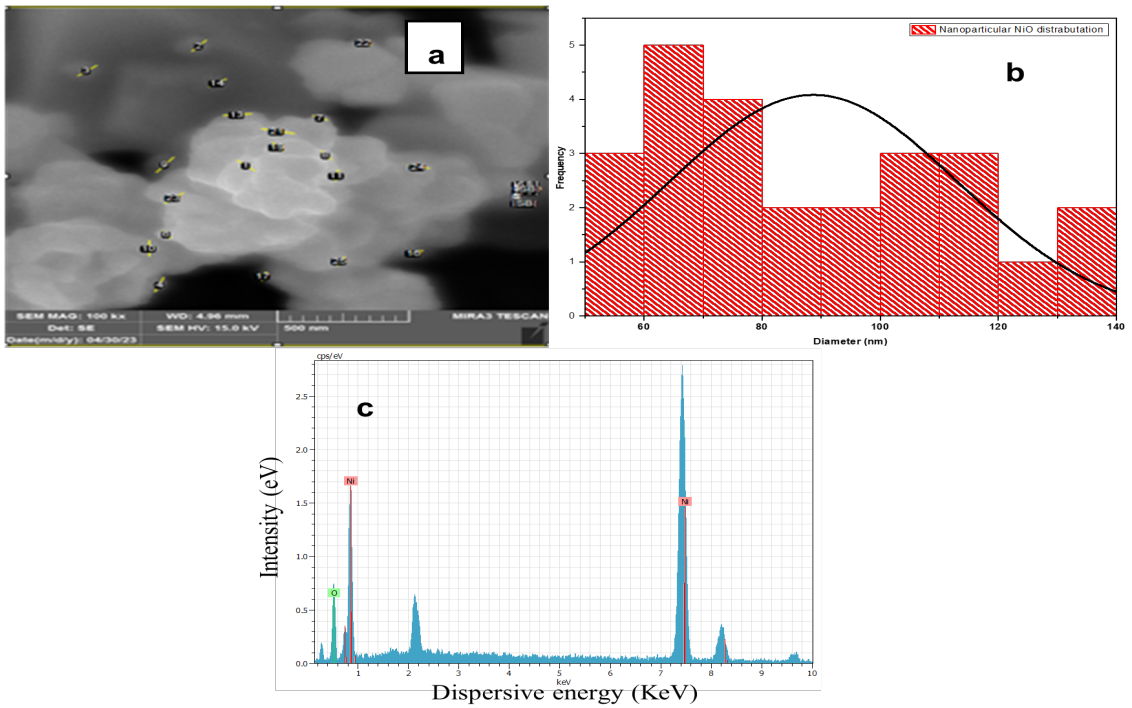

Figure 10. SEM Image for NiO Nps (b) Distribution Curve for the NiO Nps and C-EDX Spectra for NiO Nps (c)

products exhibited an average crystallite size of 22.7 nm Saadat et al. (2022), showcasing their remarkable structural characteristics.

3.6 SEM and EDX Analysis of the NiO and CuO Nanoparticles

The structural landscape and crystalline framework of the synthesized CuO and NiO hybrid nanoparticles underwent metic-

© 2024 The Authors.

Table 4. EDX Analysis of NiO and CuO Nanoparticles

Element	Mass %	Atomic %
Ni 28 K-series	40.44	56.59
O 8 K-series	8.46	43.41
Total	100	100
Cu 29 K-series	42.08	100
O 8 K-series	0.00	0.00
Total	100	100

ulous characterization by SEM, as depicted in Figures (9b and 10a). In this visual representation, the SEM images reveal the unique morphology of the calcinated CuO and NiO NP samples.

In this context, the CuO and NiO NPs appear as irregularly shaped aggregates, with their crystals dispersed in a spontaneous and aesthetically pleasing arrangement. The CuO and NiO NP samples underwent a remarkable transformation after being calcinated. They turned into smaller and rounder crystals of CuO and NiO that were evenly and smoothly distributed. This transformation, attributed to the calcination process, not only imbues the nanoparticles with aesthetic properties but also enhances their surface area, an important characteristic in catalysis. However, the histograms shown in Figures (9a and 10b) indicate that the main particle sizes of the CuO and NiO NPs formed by the thermal decomposition method at a temperature of 500°C for 6 hours are approximately 30 to 90 nm.Further evidence of the elemental composition emerged through the analysis of EDX spectra, as shown in Figures (9c and 10c) from both samples. These spectral results in Table (4) showed the presence of elemental triumvirates of Cu, Ni, and O within the CuO and NiO hybrid nanoparticles (Şenocak and İmamoğlu, 2022; Taferguennit et al., 2022).

4. CONCLUSION

In the current study, we successfully synthesized a binary metal ion Schiff base complex using salicylaldehyde and phenylethylamine in conjunction with metal acetate. The characteristics of the formed M(II) complex were determined using a comprehensive array of analytical techniques which confirmed the formation of the Schiff base ligand and the metal ion in a 1:1 molar ratio. According to the analyses conducted, the Ni complex displayed a distorted octahedral molecular structure, whereas the Cu complex demonstrated a square planar geometry. The thermal decomposition of the Ni(II) and Cu(II) Schiff base complexes led to the production of NiO and CuO nanoparticles. Moreover, XRD analysis confirmed the presence of the resultant nanoparticles, with average particle sizes of approximately 26.7 nm and 22.7 nm, respectively. The NiO nanoparticles exhibited a polycrystalline monoclinic structure, while the CuO nanoparticles displayed a cubic structure. No impurity phases were observed in either case, indicating a uniform formation of the nanoparticles.

5. ACKNOWLEDGEMENT

We are grateful to the University of Babylon, the College of Science for Women, and the University of Baghdad, Iraq for their generous support and facilities. Our institutions have been instrumental in making this research possible.

REFERENCES

Abu-Dief, A. M. and W. Mohamed (2017). α-Bi_2O_3 Nanorods: Synthesis, Characterization and UV-Photocatalytic Activity. *Materials Research Express*, **4**(3); 035039

Abu-Dief, A. M., I. F. Nassar, and W. H. Elsayed (2016). Magnetic $NiFe_2O_4$ Nanoparticles: Efficient, Heterogeneous and Reusable Catalyst for Synthesis of Acetylferrocene Chalcones and Their Anti-Tumour Activity. *Applied Organometallic Chemistry*, **30**(11); 917–923

Ali, M. A. E. A. A. and A. M. Abu-Dief (2015). $CuFe_2O_4$ Nanoparticles: An Efficient Heterogeneous Magnetically Separable Catalyst for Synthesis of Some Novel Propynyl-1H-Imidazoles Derivatives. *Tetrahedron*, **71**(17); 2579–2584

Bayansal, F., S. Kahraman, G. Çankaya, H. Çetinkara, H. Güder, and H. Çakmak (2011). Growth of Homogenous CuO Nano-Structured Thin Films by a Simple Solution Method. *Journal of Alloys and Compounds*, **509**(5); 2094–2098

Chandra, S. and L. K. Gupta (2004). EPR and Electronic Spectral Studies on Co (II), Ni (II) and Cu (II) Complexes with a new Tetradentate [N4] Macrocyclic Ligand and Their Biological Activity. *Spectrochimica Acta Part A: Molecular and Biomolecular Spectroscopy*, **60**(7); 1563–1571

Dabhane, H., S. Ghotekar, M. Zate, K.-Y. A. Lin, A. Rahdar, B. Ravindran, D. Bahiram, C. Ingale, B. Khairnar, and D. Sali (2023). A Novel Approach toward the Bio-Inspired Synthesis of CuO Nanoparticles for Phenol Degradation and Antimicrobial Applications. *Biomass Conversion and Biorefinery*; 1–16

Devi, J., S. Kumar, B. Kumar, S. Asija, and A. Kumar (2022). Synthesis, Structural Analysis, in Vitro Antioxidant, Antimicrobial Activity and Molecular Docking Studies of Transition Metal Complexes Derived from Schiff Base Ligands of 4-(Benzyloxy)-2-Hydroxybenzaldehyde. *Research on Chemical Intermediates*, **48**(4); 1541–1576

Devi, P., K. Singh, and B. Kubavat (2023). Synthesis, Spectroscopic, Quantum, Thermal and Kinetics, Antibacterial and Antifungal Studies: Novel Schiff Base 5-Methyl-3-((5-Bromosalicylidene) Amino)-Pyrazole and Its Transition Metal Complexes. *Results in Chemistry*, **5**; 100813

Elseman, A. M., D. Rayan, and M. Rashad (2016). Structure, Optical and Magnetic Behavior of Nanocrystalline CuO Nanopowders Synthesized Via a New Technique Using Schiff Base Complex. *Journal of Materials Science: Materials in Electronics*, **27**; 2652–2661

Farhadi, S. and Z. Roostaei-Zaniyani (2011). Simple and

© 2024 The Authors.

Low-Temperature Synthesis of NiO Nanoparticles through Solid-State Thermal Decomposition of the Hexa (ammine) Ni (ii) Nitrate, $[Ni(NH_3)_6](NO_3)_2$, Complex. *Polyhedron*, **30**(7); 1244–1249

Ghaffari, A., M. Behzad, M. Pooyan, H. A. Rudbari, and G. Bruno (2014). Crystal Structures and Catalytic Performance of Three New Methoxy Substituted Salen Type Nickel (II) Schiff Base Complexes Derived from Meso-1, 2-Diphenyl-1, 2-Ethylenediamine. *Journal of Molecular Structure*, **1063**; 1–7

Gobinath, E., M. Dhatchinamoorthy, P. Saran, D. Vishnu, R. Indumathy, and G. Kalaiarasi (2023). Synthesis and Characterization of NiO Nanoparticles Using Sesbania Grandiflora Flower to Evaluate Cytotoxicity. *Results in Chemistry*, **6**; 101043

Gopalan, R. (2001). *Concise coordination chemistry*. Vikas publishing house

Hossain, A. M. S., J. M. Méndez-Arriaga, C. Xia, J. Xie, and S. Gómez-Ruiz (2022). Metal Complexes with ONS Donor Schiff Bases. A Review. *Polyhedron*, **217**; 115692

Ibrahim, E., L. H. Abdel-Rahman, A. M. Abu-Dief, A. Elshafaie, S. K. Hamdan, and A. Ahmed (2018). The Synthesis of CuO and NiO Nanoparticles by Facile Thermal Decomposition of Metal-Schiff Base Complexes and an Examination of Their Electric, Thermoelectric and Magnetic Properties. *Materials Research Bulletin*, **107**; 492–497

Jassim, S. M., M. A. Abd, and I. A. Hammed (2023). Green Synthesis of Nickel Oxide Nanoparticles Using Syzygium Aromatic Extract: Characterization and Biological Applications. *Al-Bahir Journal for Engineering and Pure Sciences*, **2**(2); 7

Jeewoth, T., H. Li Kam Wah, M. G. Bhowon, D. Ghoorohoo, and K. Babooram (2000). Synthesis and Anti-Bacterial/catalytic Properties of Schiff Bases and Schiff Base Metal Complexes Derived from 2, 3-Diaminopyridine. *Sythesis and Reactivity in Inorganic and Matel-Organic Chemistry*, **30**(6); 1023–1038

Jia, W., E. Reitz, P. Shimpi, E. G. Rodriguez, P.-X. Gao, and Y. Lei (2009). Spherical CuO Synthesized by a Simple Hydrothermal Reaction: Concentration-Dependent Size and Its Electrocatalytic Application. *Materials Research Bulletin*, **44**(8); 1681–1686

Kargar, H., A. Adabi Ardakani, K. S. Munawar, M. Ashfaq, and M. N. Tahir (2021). Nickel (II), Copper (II) and Zinc (II) Complexes Containing Symmetrical Tetradentate Schiff Base Ligand Derived from 3, 5-Diiodosalicylaldehyde: Synthesis, Characterization, Crystal Structure and Antimicrobial Activity. *Journal of the Iranian Chemical Society*, **18**; 2493–2503

Khalaji, A. D. (2013). Preparation and Characterization of NiO Nanoparticles Via Solid-State Thermal Decomposition of Nickel (II) Schiff Base Complexes [Ni (salophen)] and [Ni (me-Salophen)]. *Journal of Cluster Science*, **24**(1); 209–215

V. Kuchtanin, L. Kleščíková, M. Šoral, R. Fischer, Z. Ružičková, E. Rakovský, J. Moncol', dan P. Segl'a (2016). Nickel (II) Schiff base complexes: Synthesis, characterization and catalytic activity in Kumada–Corriu cross-coupling reactions. *Polyhedron*, **117**, 90–96.

Nakamoto, K. (2009). *Infrared and Raman Spectra of Inorganic and Coordination Compounds, Part B: Applications in Coordination, Organometallic, and Bioinorganic Chemistry*. John Wiley & Sons

Ourari, A., Y. Ouennoughi, D. Aggoun, M. S. Mubarak, E. M. Pasciak, and D. G. Peters (2014). Synthesis, Characterization, and Electrochemical Study of a New Tetradentate Nickel (II)-Schiff Base Complex Derived from Ethylenediamine and 5'-(N-Methyl-N-Phenylaminomethyl)-2'-Hydroxyacetophenone. *Polyhedron*, **67**; 59–64

Parashar, R., R. Sharma, A. Kumar, and G. Mohan (1988). Stability Studies in Relation to IR Data of Some Schiff Base Complexes of Transition Metals and Their Biological and Pharmacological Studies. *Inorganica chimica acta*, **151**(3); 201–208

Parveen, K., V. Banse, and L. Ledwani (2016). Green Synthesis of Nanoparticles: Their Advantages and Disadvantages. In *AIP Conference Proceedings*, volume 1724. AIP Publishing

Patterson, A. (1939). The Scherrer Formula for X-Ray Particle Size Determination. *Physical review*, **56**(10); 978

Phurat, C., T. Teerawatananond, and N. Muangsin (2010). 2-[(4-Chlorobenzyl) Iminomethyl] Phenol. *Acta Crystallographica Section E: Structure Reports Online*, **66**(9); o2310–o2310

Refat, M. S., H. A. Saad, A. A. Gobouri, M. Alsawat, A. M. A. Adam, and S. M. El-Megharbel (2022). Charge Transfer Complexation between Some Transition Metal Ions with Azo Schiff Base Donor As a Smart Precursor for Synthesis of Nano Oxides: An Adsorption Efficiency for Treatment of Congo Red Dye in Wastewater. *Journal of Molecular Liquids*, **345**; 117140

Saadat, A., A. Banaei, P. Mcardle, R. Jafari (2022). Spectral, Structural, and Antibacterial Study of Copper (II) Complex with N_2O_2 Donor Schiff Base Ligand and Its Usage in Preparation of CuO Nanoparticles. *Journal of Chemistry*, **2022**; 1–13

Salavati-Niasari, M., N. Mir, and F. Davar (2009a). Synthesis and Characterization of NiO Nanoclusters Via Thermal Decomposition. *Polyhedron*, **28**(6); 1111–1114

Salavati-Niasari, M., F. Mohandes, F. Davar, M. Mazaheri, M. Monemzadeh, and N. Yavarinia (2009b). Preparation of NiO Nanoparticles from Metal-Organic Frameworks Via a Solid-State Decomposition Route. *Inorganica Chimica Acta*, **362**(10); 3691–3697

Santhi, S., R. Renganathan, S. Amala, G. Suganya, and K. Abinaya (2023). Highly Selective and Sensitive Dual Channel New Schiff Base Chemosensor Based on 5-Bromo-2-Hydroxybenzaldehyde and Its Co (II), Ni (II), Cu (II) and Zn (II) Complexes-Synthesis, Spectral and Theoretical Characterization and Pharmacological Applications. *Vietnam Journal of Chemistry*, **61**(4); 429–444

© 2024 The Authors.

Şenocak, A. and R. İmamoğlu (2022). NiO nanoparticles via calcination of a Schiff base complex: Photocatalytic and microbicidal activity

Silverstein, R., F. Webster, and D. Kiemle (2005). Silverstein-Spectrometric Identification of Organic Compounds 7th Ed. *The State University of New York, College of Environmental Science and Forestry*

Singh, A., H. P. Gogoi, and P. Barman (2023). Synthesis of Metal Oxide Nanoparticles by Facile Thermal Decomposition of New Co (II), Ni (II), and Zn (II) Schiff Base Complexes-Optical Properties and Photocatalytic Degradation of Methylene Blue Dye. *Inorganica Chimica Acta*, **546**; 121292

Singh, P. K. and D. N. Kumar (2006). Spectral Studies on Cobalt (II), Nickel (II) and Copper (II) Complexes of Naphthaldehyde Substituted Aroylhydrazones. *Spectrochimica Acta Part A: Molecular and Biomolecular Spectroscopy*, **64**(4); 853–858

Sumalatha, V., D. Ayodhya, and V. Balchander (2023). Facile Synthesis of Hexagonal-Shaped CuO NPs from Cu (ii)-Schiff Base Complex for Enhanced Visible-Light-Driven Degradation of Dyes and Antimicrobial Studies. *Inorganica Chimica Acta*, **548**; 121358

Taferguennit, M., N. Kichou, N. Guechtouli, and H. Zakia (2022). CuO Nanoparticls Thermally Synthesized from a Since-Wheel Copper (II) Complex. *The Eurasia Proceedings of Science Technology Engineering and Mathematics*, **20**; 43–48

Tsacheva, I., Z. Todorova, D. Momekova, G. Momekov, and N. Koseva (2023). Pharmacological Activities of Schiff Bases and Their Derivatives with Low and High Molecular Phosphonates. *Pharmaceuticals*, **16**(7); 938

Turner, J. F. (2002). Ligand Field Theory and Its Applications (Figgis, Brian N.; Hitchman, Michael A.). *Journal of Chemical Education*, **79**(9); 1072

Yang, C., X. Su, J. Wang, X. Cao, S. Wang, and L. Zhang (2013). Facile Microwave-Assisted Hydrothermal Synthesis of Varied-Shaped CuO Nanoparticles and Their Gas Sensing Properties. *Sensors and Actuators B: Chemical*, **185**; 159–165

Yousif, E., A. Majeed, K. Al-Sammarrae, N. Salih, J. Salimon, and B. Abdullah (2017). Metal Complexes of Schiff Base: Preparation, Characterization and Antibacterial Activity. *Arabian Journal of Chemistry*, **10**; S1639–S1644

© 2024 The Authors.